ARTICLE

OBC
www.rsc.org/obc

Solid state NMR studies and density functional theory (DFT) calculations of conformers of quercetin†

Sebastian Olejniczak and Marek J. Potrzebowski*
Polish Academy of Sciences, Department of Structural Studies and NMR Laboratory, Centre of Molecular and Macromolecular Studies, Sienkiewicza 112, 90-363 Łódź, Poland.
E-mail: marekpot@bilbo.cbmm.lodz.pl

Received 7th May 2004, Accepted 17th June 2004
First published as an Advance Article on the web 27th July 2004

This work presents the first comparative analysis of two crystallographic modifications of quercetin (3,3′,4′,5,7-pentahydroxyflavone). The existence of dihydrate and unhydrated forms of quercetin in the solid state is confirmed by several experimental techniques *e.g.* X-ray diffraction of powders, DSC, TGA, and NMR. Our studies allow an understanding of the complexity of quercetin samples obtained from different sources. A PASS-2D experiment is employed to establish principal values of ^{13}C chemical shift tensors for both modifications. Solid state NMR spectroscopy and DFT GIAO calculations provide unique information about NMR shielding and electron density distribution for different conformers. It has been concluded that changes of conformation and hydrogen bonding pattern have great influence on bond order parameters of quercetin. Theoretical calculations and experimental data do not exclude the existence of the *syn* conformer of quercetin, which so far was not considered in the condensed phase.

Introduction

Much attention has been given to physiological and structural studies of quercetin (3,3′,4′,5,7-pentahydroxyflavone) (Scheme 1), one of the most important compounds belonging to the flavonoid group. The literature on quercetin is growing rapidly, a database search having produced over 3000 references in the last seven years alone. The interest in this natural product, found in many plant materials is related to its role in vital processes. Ouercetin and other flavonoids have been shown to modify *anti*-prostanoid and *anti*-inflammatory responses, protect low-density lipoprotein from oxidation and promote relaxation of cardiovascular smooth muscle. Moreover, many of the flavonoids play a role as antioxidants, scavengers of free radicals. The biology of quercetin and related bioflavonoids has been exhaustively reviewed.[1,2]

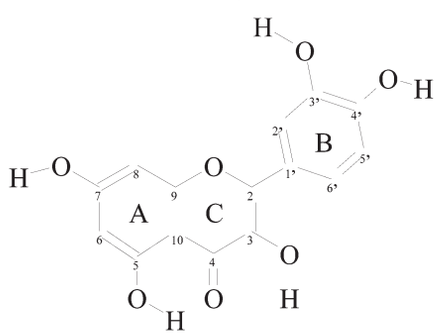

Scheme 1

The quercetin has been intensively investigated by means of theoretical methods in order to establish the most stable conformation and conclude the relationship between the structure and biological activity. These studies were carried out on different level of theory. Russo *et al.* employing semiempirical AM1 and PM3 methods revealed that quercetin has a nonplanar molecular structure, with cross-conjugation occurring at the C ring.[3] Later on Erkoç and coworkers, using the same AM1 method, showed the planar geometry of quercetin and its radical isomers.[4] The *ab initio* calculation at the RHF level with the STO-3G basis set did not provide convincing evidence to allow the geometry of quercetin to be equivocally concluded.[5] Vasilescu and Girma, employing the higher level basis set 6-31G* revealed that the rotation of the B ring with regard to the C ring is very easy in the range of torsional angle O1–C2–C1′–C6′ equal to 0°–30° and 150°–180°.[6] Very recently, Toscano and coworkers published the first density functional theory (DFT) calculations of quercetin with the B3LYP functional and 6-311++G** basis set.[7] It should be expressed that in quoted work geometry optimization and conformational analysis were computed including also the effect of the environment. Moreover, it was shown that the theoretical approach can be employed to establish ESR spectral parameters and explain experimental spectroscopic properties in vacuum and liquid phase.

Less attention was paid to structural studies of quercetin in the condensed phase, nonetheless despite of difficulties to obtain suitable crystals for X-ray studies, the crystal and molecular structure of quercetin was established.[8] In the solid phase quercetin crystallizes as the dihydrate in a fairly planar conformation with molecular geometry as shown in Scheme 1. In this paper employing high resolution solid state NMR studies and theoretical DFT calculations of ^{13}C shielding parameters we consider the presence in the condensed phase of a second conformer of quercetin with a planar conformation of the aromatic rings and the opposite arrangement of the B ring (*syn* geometry of the hydroxyl groups at C3 and C3′ atoms). The influence of inter- and intramolecular hydrogen bonding on the change of NMR parameters is also discussed.

Results

^{13}C Solid state NMR, X-ray of powder diffraction and DSC studies

The preliminary ^{13}C CP/MAS NMR studies of quercetin performed with sample spinning at 3.5 kHz were published by Wawer and Zielińska.[9] The quercetin was obtained from plants by hydrolysis of quercetin glycosides isolated from the lily of the valley herb (*Convallaria majalis*) and the St-John's-wort herb (*Hypericum perforatum*). The structure assignment was done by comparison of ^{13}C isotropic chemical shifts in liquid (solution in DMSO) and solid phases. In our projects we used commercial samples, purchased from Aldrich (sample **1**) and ICN Biomedicals (sample **2**). Both samples specified as quercetin·dihydrate were investigated as supplied, without purification and recrystallization. ^{13}C CP/MAS spectra of **1** and **2** recorded at 7 kHz with RAMP shape cross-polarization[10] and TPPM[11] decoupling are shown in Fig. 1.

From comparison of spectra, the distinction in chemical shifts, intensities of signals, splitting between lines, it is apparent that

† Electronic supplementary information (ESI) available: TGA profiles for samples **1** and **2** and ^{13}C NMR shielding parameters. See http://www.rsc.org/suppdata/ob/b4/b406861k/

DOI: 10.1039/b406861k

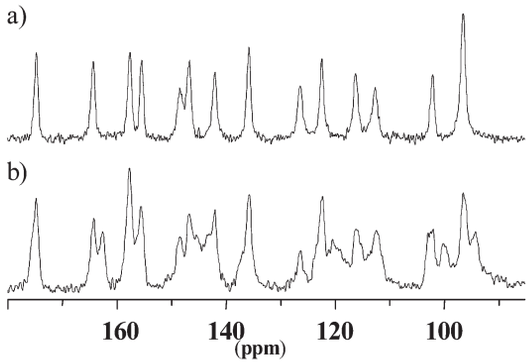

Fig. 1 75.46 MHz ^{13}C CP/MAS NMR spectra of quercetin recorded at 7 kHz with RAMP shape cross-polarization and TPPM decoupling a) sample 1, b) sample 2.

samples of **1** and **2** are significantly different. On the other hand, ^{13}C NMR spectra of samples dissolved in DMSO show exactly the same pattern what proves that from chemical point of view **1** and **2** are identical. In order to explain distinction causes by so called "solid state effects" in the next step the thermal analysis of samples was done. Fig. 2 presents the DSC profiles for both samples. TGA curves are available as supplementary material.† Analysis of the data clearly shows similarities and differences between **1** and **2**. Both samples show strong endothermic peaks corresponding to release of water from the crystal lattice. The temperature is much higher than the boiling point of water which means that molecules of water are strongly held by the quercetin *via* hydrogen bonding. The minute difference in temperatures of water evaporation and its heat of release is noteworthy. However the most significant distinction is found for the melting points, which for sample **1** is equal to 324.1 °C (Fig. 2a) while for sample **2** two peaks at 319.5 °C and 323.5 °C are apparent (Fig. 2b). Such a result, suggest that in the case of sample **2** we have a mixture of different forms. This conclusion is consistent with TGA studies. For sample **1** the loss of weight related to evaporation of solvent is 10.77% while for **2** it is only 7.0%. The former value very well corresponds to the theoretical value (10.64%) of the well defined dihydrate. The sample **2** is mixture of dihydrate or monohydrate and/or unhydrated form.

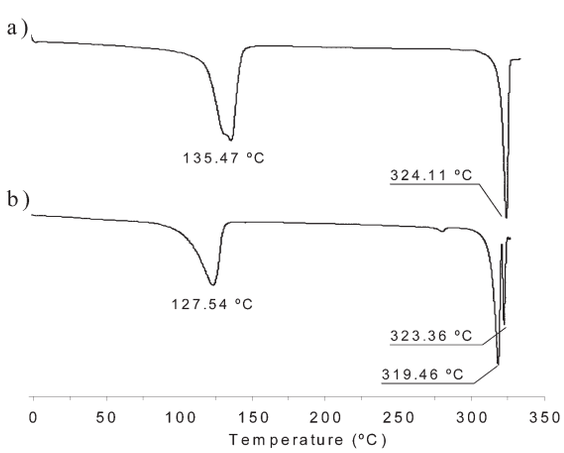

Fig. 2 DSC profiles for a) sample **1**, b) sample **2**.

Much effort was paid to find crystallization conditions for the preparation of unhydrated quercetin. Fig. 3a shows ^{13}C CP/MAS spectrum of sample **3** crystallized two times from methanol. The DSC profile of **3** shown in Fig. 3b clearly proves the lack of water in the crystal lattice. The melting temperature is 319.3 °C, very close to value one of the components seen in Fig. 2b.

In order to simplify the assignment of structures and highlight differences between **1** and **3** we performed a dipolar dephasing (DD) experiment.[12] This method is often used as a spectral editing technique. In the simplest approach after CP, the ^{1}H decoupler is turned off for *ca.* 50 μs. This is sufficient time for ^{13}C–^{1}H dipolar coupling to dephase the transverse magnetization for any

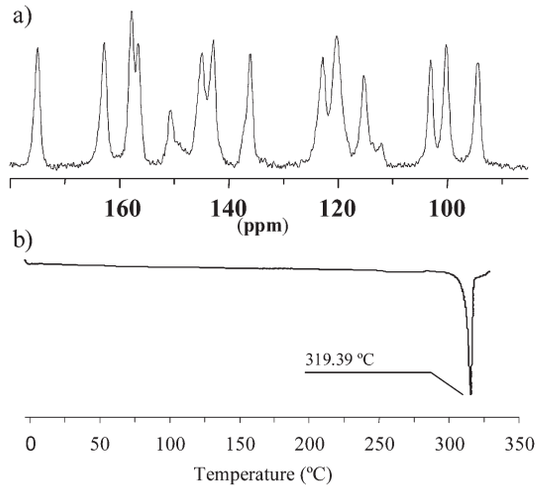

Fig. 3 a) 75.46 MHz ^{13}C CP/MAS NMR spectrum of sample **3**, recorded at 7 kHz with RAMP shape cross-polarization and TPPM decoupling. b) DSC profile for sample **3**.

^{13}C with a directly bonded ^{1}H, as long as the dipolar coupling is not motionally averaged. Therefore the lines for rigid CH are effectively suppressed. The quercetin consists of fifteen carbon atoms, ten quaternary and five CH. The CP/MAS spectra (Fig. 1a and 3a) display only 14 isotropic signals because of the overlap effect. Fig. 4 shows the DD spectra of **1** and **3** with τ_D equal to 50 μs. As seen the intensity of methine signals is reduced to zero and in consequence ten quaternary carbons are observed. It means that for both crystallographic forms one of the CH atoms overlaps the signal of a quaternary carbon.

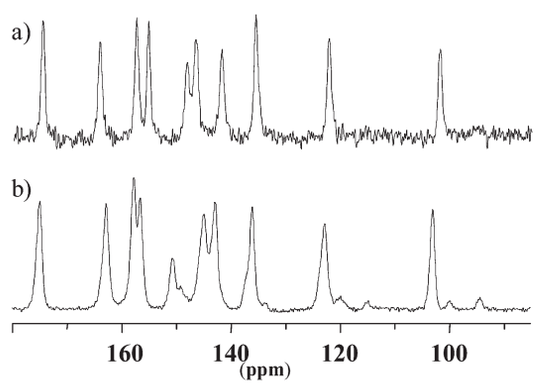

Fig. 4 75.46 MHz ^{13}C NMR dipolar dephasing MAS spectra recorded at a spinning rate of 7 kHz with τ_D equal to 50 μs a) sample **1**, b) sample **3**.

It is interesting to note that the crystal lattices of sample **1** and **3** are different. Fig. 5 shows the X-ray powder diffraction pattern for **1** and **3** (Fig. 5a and Fig. 5b respectively). The pattern calculated from the refined structure of **1** is compared to the X-ray diffraction raw data pattern for the assessment of the correct crystal structure determination (Fig. 5c). Comparing the computed and observed molecular properties provided verification of the structure.

GIAO calculations of ^{13}C NMR parameters

The distinction of the crystal structure related with the number of water molecules in the lattice has significant influence on isotropic chemical shifts of quercetin. The assignment of structure is not a trivial task and an approach based on a simple comparison of isotropic lines in liquid and solid phases can lead to misleading information. The most challenging question about the refinement of **1** and **3** regards the origin of the observed distinction of ^{13}C δ_{iso} values and its correlation with intramolecular effects (*e.g.* change of conformation) and/or intermolecular contacts (*e.g.* hydrogen bonding, aromatic–aromatic stacking). In order to answer these questions, in this section we have carried out theoretical calculations of NMR shielding parameters considering intramolecular interactions.

Table 1 Influence of Θ_2 torsional angles (180° and 0°) on ^{13}C NMR shielding parameters of *anti* and *syn* conformers of quercetin[a]

	anti (Θ_1 = 180°)								***syn*** (Θ_1 = 0°)							
	σ_{iso} (ppm)		σ_{11} (ppm)		σ_{22} (ppm)		σ_{33} (ppm)		σ_{iso} (ppm)		σ_{11} (ppm)		σ_{22} (ppm)		σ_{33} (ppm)	
	I	**III**	**I**	**III**	**I**	**III**	**I**	**III**	**II**	**IV**	**II**	**IV**	**II**	**IV**	**II**	**IV**
C2	40.1	39.9	−25	−25	40	40	105	105	40.0	40.0	−25	−25	40	40	105	105
C3	46.5	46.3	−3	−3	19	19	123	123	47.1	46.4	−1	−3	20	19	122	123
C4	12.4	12.2	−58	−59	−18	−19	114	114	12.3	12.0	−58	−59	−18	−18	114	114
C5	19.3	19.4	−54	−54	−1	−1	113	113	19.4	19.3	−54	−54	−1	−1	113	113
C6	88.4	88.4	31	31	87	87	147	147	88.4	88.5	31	31	87	87	147	147
C7	20.2	20.1	−66	−66	8	7	119	119	20.1	20.2	−66	−66	7	8	119	119
C8	92.1	91.5	35	34	84	82	158	158	91.8	91.9	35	35	83	83	158	158
C9	27.2	27.1	−48	−48	16	16	113	113	27.0	27.0	−48	−48	16	16	113	114
C10	82.5	82.6	19	19	53	53	175	175	82.5	82.4	19	19	53	53	175	175
C1′	59.9	57.6	−20	−25	41	39	159	159	60.0	57.9	−21	−25	42	39	160	160
C2′	73.1	71.0	−6	−8	**66**	**51**	159	170	68.3	66.2	−6	−8	**54**	**39**	157	168
C3′	37.6	37.3	−29	−30	22	20	120	121	37.7	37.3	−29	−30	22	20	120	122
C4′	35.6	39.1	−29	−27	16	23	120	121	35.7	39.2	−29	−26	15	23	120	121
C5′	69.3	72.1	−14	−10	68	68	154	158	69.8	72.6	−13	−10	68	69	154	159
C6′	60.0	61.4	−31	−28	**36**	**37**	176	176	65.2	66.7	−30	−27	**48**	**49**	178	178

[a] Upper case Roman numerals correspond to structures shown in Scheme 2.

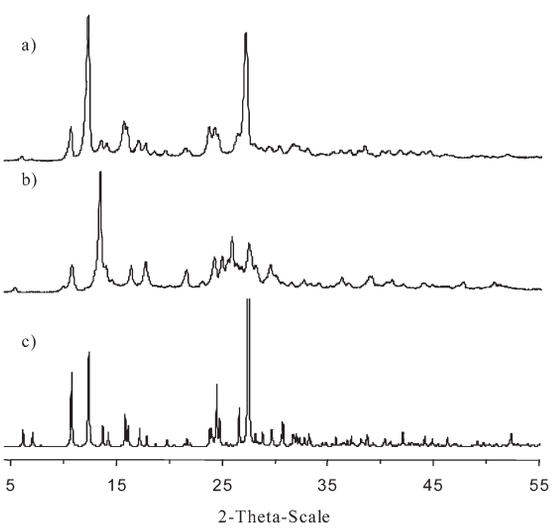

Fig. 5 X-Ray diffraction powder pattern for a) sample **1**, b) sample **3**. Trace c presents a theoretical diffractogram taking coordinates from ref. 8.

A number of methods are currently available for computing of NMR parameters.[13,14] In our work, the GIAO B3PW91 hybrid method and 6-311G** basis set was used for the calculation of the ^{13}C parameters employing the Gaussian program.[15] Quercetin with fully optimized geometry has been computed. To test the influence of intramolecular effects on NMR shielding we considered different conformers of quercetin. First, we dealt with conformers in a planar arrangement of A, B and C rings, *anti* and *syn* orientation of hydroxyl groups at 3 and 3′ carbon atoms. The appropriate Θ_1 torsional angles defined as O1–C2–C1′–C6′ are 180° and 0° (see Scheme 2). In the next step, *anti* and *syn* models with changed arrangement of hydroxyl groups at C3′ and C4′ were computed. In such an alignment the hydroxyl residues are involved in intramolecular hydrogen bonding. The appropriate Θ_2 torsion angle defined as H3′–O3′–C3′–C4′ is 180° and 0°, respectively. For Θ_2 of 0° the distance between H3′ and O4′ oxygen is 2.127 Å. Comparing the energy for each conformer it is apparent that intramolecular hydrogen bonding has stabilization effect and for samples with Θ_2 equal to 0° the energy is slightly lower. However, the most important information regards the distinction of ^{13}C σ_{iso} for C2′ and C6′ atoms. GIAO calculations reveal that for *syn* conformation with Θ_2 of 0° the difference in chemical shifts is very small (0.5 ppm) while for *anti* geometry disparity of 9.5 ppm is observed. It is interesting to note that for the *syn* conformer and opposite alignment of hydrogens with Θ_3 (H–O4′–C4′–C3′) equal to 0° and Θ_2 equal to 180°, the distinction

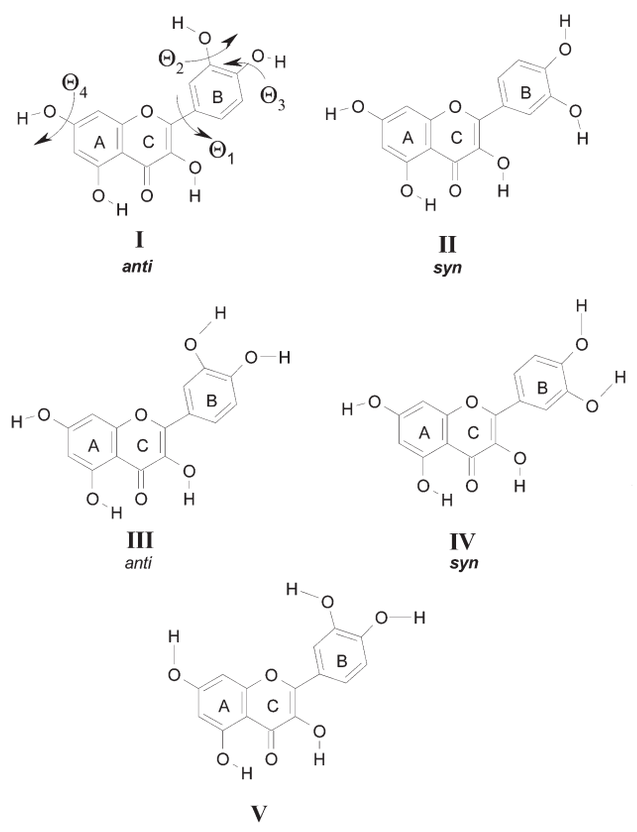

Scheme 2

of ^{13}C σ_{iso} parameters for C2′ and C6′ is very large, −18.2 ppm (see supplementary material†).

The obtained values of shielding parameters are collected in Table 1. Fig. 6 displays the correlation of experimental ^{13}C δ_{iso} *versus* theoretical ^{13}C σ_{iso} values. The elucidation of ^{13}C δ_{iso} shifts was done by regression procedure and choice the best-fitted parameters. The cross-correlated assignments gave the worse fitting of data. On the basis of the CP/MAS and DD/MAS experiments as well as theoretical calculations we propose the assignment presented in pictorial form in Fig. 7. It should be stressed that our assignment for sample **1** is only slightly different compared to that reported elsewhere.[9]

Experimental data (Fig. 7) show that the most significant distinction between **1** and **3** is found for carbons 2′, 6′ (ring B) and carbons 6 and 8 (ring A). For **1** the difference between ^{13}C δ_{iso} of

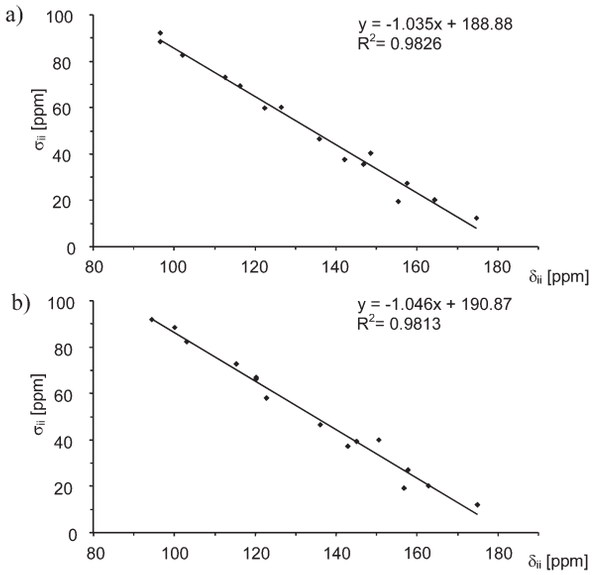

Fig. 6 Correlation between isotropic values of experimental ^{13}C chemical shifts and theoretical shielding, a) plot for sample **1** and structure **I**. b) plot for sample **3** and structure **IV**.

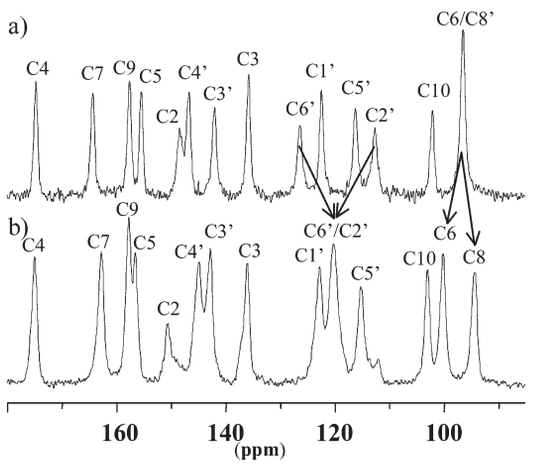

Fig. 7 Assignment of structure for a) sample **1**, b) sample **3**. Numbers correspond to carbon atoms according to Scheme 1. Arrows show shift of appropriate carbons.

C2′ and C6′ is equal to −13.6 ppm and between C6 and C8 equal to 0.1 ppm. The appropriate values for **3** are 0.0 ppm and 5.9 ppm, respectively. It has to be stressed that theoretical calculations for *anti* and *syn* conformers (Table 1) correspond well to experimental data for C2′ and C6′ and clearly prove the distinction of isotropic values in the function of Θ_1 and Θ_2 torsional angle. On the other hand, from GIAO calculations it is apparent that the change of conformation of quercetin considering different values of Θ_1, Θ_2, Θ_3 angles has only a small influence on shielding of the C6 and C8 carbon atoms of the A ring.

So far, for all conformers the Θ_4 angle defined as H–O7–C7–C8 was equal to 180° and the observed difference is *ca.* 4 ppm. In order to conclude the influence of intramolecular effects on NMR shielding parameters, the model with Θ_4 equal to 0° was computed. The calculated values (Table 2) revealed a significant distinction between the C6 and C8 atoms, which for this conformer is found to be 9.0 ppm.

Changing parameters, which characterize the intramolecular geometry in any case, we did not find a conformation showing the lack of distinction of NMR parameters for C6 and C8 carbons. We assume that for those atoms intermolecular interactions, *e.g.* hydrogen bonding are responsible for reducing the disparity. From the discussion it is apparent that cluster type calculations including water molecules and geometry established by diffraction techniques will provide a better description of changes of NMR shielding. This problem is discussed in the next section.

Table 2 Influence of Θ_4 torsional angles on ^{13}C NMR shielding parameters of quercetin[a]

anti with $\Theta_4 = 0°$ **(V)**

	σ_{iso} (ppm)	σ_{11} (ppm)	σ_{22} (ppm)	σ_{33} (ppm)
C2	40.6	−24	41	105
C3	46.2	−3	19	123
C4	12.5	−59	−18	114
C5	18.9	−55	−1	113
C6	85.8	26	75	156
C7	20.0	−66	8	118
C8	94.8	39	96	149
C9	27.7	−47	16	114
C10	82.3	20	52	175
C1′	59.9	−20	41	159
C2′	73.5	−5	67	159
C3′	37.7	−29	22	120
C4′	35.7	−29	16	120
C5′	69.2	−14	67	154
C6′	60.1	−31	36	176

[a] Upper case Roman numerals correspond to structure shown in Scheme 2.

Analysis of ^{13}C chemical shift tensor (CST) parameters

It is well known that detailed information about the electronic surrounding of each nucleus, which reflects subtle structural effects and intermolecular interactions, can be obtained from inspection of the tensorial nature of the chemical shift. Hence, in this part of the project we were attracted by the prospect of analysis of ^{13}C δ_{ii} data for **1** and **3**, inspection of anisotropic values of chemical shift tensors and correlation of the principal elements to the molecular structure. For rotating solids, ^{13}C δ_{ii} parameters can be obtained from the analysis of spinning side-band intensities. For the samples under investigation, the spinning rate should be in range of 2–3 kHz, to obtain a spectrum with a sufficient number of sidebands for further calculations of the aromatic region. As we found in the case of **1** and **3** the deconvolution procedure is not an easy task. At a low spinning speed the overlap between different spinning sidebands manifolds and analysis of the spectrum is ambiguous.

The separation of the isotropic and anisotropic part of the spectra with heavy overlapped systems is still a challenge for solid state NMR spectroscopy. There are several approaches, which allow this goal to be achieved.[16] In our project we employed the PASS 2D sequence, which compared to other techniques offers good sensitivity and does not require any hardware modifications or special probehead. A detailed explanation on the PASS-2D pulse sequence, its performance, a Mathematica routine to generate a set of PASS solutions, and the data processing can be found elsewhere.[17,18]

Fig. 8a displays the PASS-2D spectrum of **1**, recorded with a spinning rate of 2 kHz. The aromatic atoms are characterized by large CSA and under slow sample spinning the spectrum presents a complex pattern. Distortion of the 2-D spectrum is removed by its tilting about the proper angle (in this case −53.1°) along the horizontal through the center of the matrix (Fig. 8b). Then it is possible to separate the spinning sidebands for each carbon as a F1 slice and employing the calculation procedure to establish the ^{13}C δ_{ii} parameters. It is clear from such a presentation that the F2 projection corresponds to the TOSS[19] spectrum while F1 represents CSA. In this work ^{13}C δ_{ii} values were obtained by means of the SIMPSON program.[20] A similar procedure was employed to analyse the ^{13}C CST parameters of **3**. The experimental and the best-fitting simulated 1D spinning CSA sideband pattern for compounds **1** and **3** are shown in Fig. 8c. The ^{13}C δ_{ii} parameters are collected in Table 3.

The experimental ^{13}C CST parameters were compared with theoretical data obtained by GIAO calculations. In this case, the X-ray diffraction data of **1** was taken as an input file.[7] The advantage of such an approach is related to the fact that it is possible to compare the theoretical and experimental results for molecules with exactly the same geometry of heavy atoms. In our calculations the intermolecular

Table 3 Experimental values of ^{13}C NMR chemical shift parameters for samples **1** and **3**. Theoretical values for sample **1**[a]

	Sample 1				*Sample 3*				*Sample 1*[a]			
	δ_{iso} (ppm)	δ_{11} (ppm)	δ_{22} (ppm)	δ_{33} (ppm)	δ_{iso} (ppm)	δ_{11} (ppm)	δ_{22} (ppm)	δ_{33} (ppm)	δ_{iso} (ppm)	δ_{11} (ppm)	δ_{22} (ppm)	δ_{33} (ppm)
C2	148.5	226	152	67	150.6	228	151	73	144.1	213	142	78
C3	135.8	187	159	62	136.0	185	160	63	134.8	189	155	65
C4	174.8	239	217	68	175.0	239	219	68	172.3	255	190	71
C5	155.5	233	171	62	156.7	235	171	64	161.3	234	181	69
C6	96.6	151	114	24	100.1	158	116	27	88.9	154	90	22
C7	164.4	255	178	61	162.8	252	177	60	159.9	245	171	64
C8	96.5	151	114	24	94.5	151	109	23	88.8	150	97	20
C9	157.7	238	168	68	157.8	235	168	70	157.1	231	170	71
C10	102.1	159	146	1	103.0	164	143	3	101.8	156	139	10
C1′	122.5	204	145	19	122.9	209	141	19	121.9	205	137	23
C2′	112.7	190	134	14	120.3	207	146	8	108.0	193	118	13
C3′	142.1	211	154	61	142.9	212	155	61	146.8	213	167	61
C4′	146.7	217	162	61	145.1	214	161	60	148.7	210	172	64
C5′	116.3	196	135	18	115.4	196	131	19	109.6	200	115	14
C6′	126.5	216	156	7	120.3	207	146	8	116.0	209	142	−3

[a] Theoretical values calculated with the GIAO B3PW91 hybrid method and 6-311G** basis set. The equation $\delta_{ii} = 181 - 0.99\sigma_{ii}$ ($R^2 = 0.9837$) was employed to convert shielding to chemical shift parameters.

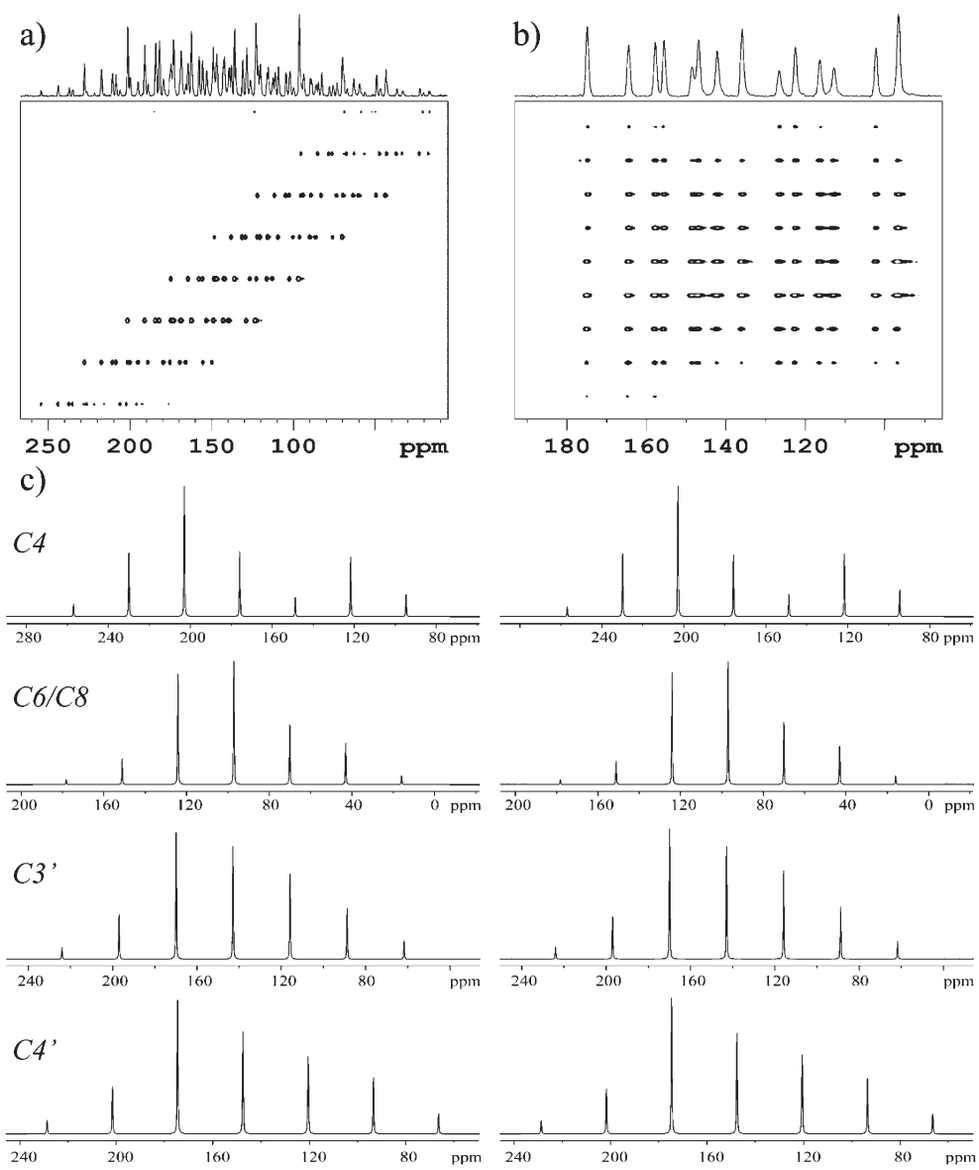

Fig. 8 PASS-2D spectrum of **1** a) recorded with spinning rate 2 kHz. b) after proper data shearing. c) the experimental (left column) and the best-fitting simulated (right column) 1D spinning CSA sideband pattern for selected carbon atoms. Experimental spectra are taken as F1 slices from Fig. 2b.

hydrogen bonding present in the crystal lattice was preserved. The position of hydrogen atoms was optimized since the X-ray diffraction often has difficulty locating protons accurately. The importance of C–H bond length optimization in GIAO computing of ^{13}C NMR parameters was discussed elsewhere.[21] The theoretical ^{13}C chemical shielding parameters calculated by means of the GIAO method for **1** are given in Table 3. Fig. 9 shows correlation of the experimental chemical shift δ_{ii} parameters of **1** *versus* the shielding parameters.

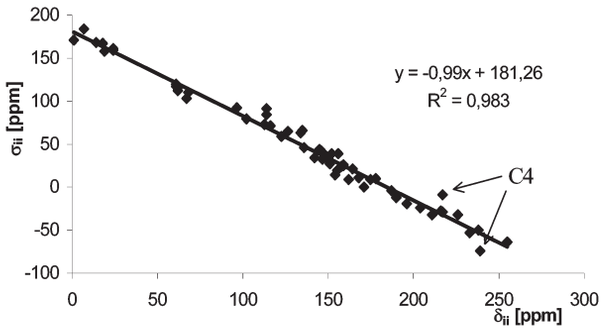

Fig. 9 Correlation between experimental values of ^{13}C chemical shifts and theoretical shielding for sample **1**.

The equation $\delta_{ii} = 181 - 0.99\sigma_{ii}$ ($R^2 = 0.9837$) was employed to convert shielding to chemical shift parameters. The values of calculated ^{13}C σ parameters for **1** clearly prove that considering the intermolecular hydrogen bonds, in particular of the hydroxyl group at the C7 atom the very small distinction of chemical shifts between C6 and C8 can be explained.

The orientation of the principal elements of chemical shift tensors with respect to the molecular structure of the aromatic compounds was exhaustively discussed by Grant.[22] Fig. 10 shows the orientation of ^{13}C δ_{ii} parameters for **1**. In principle, the δ_{11} elements are oriented along the C–H bonds while δ_{22} are aligned in the aromatic plane while δ_{33} is perpendicular to this plane.

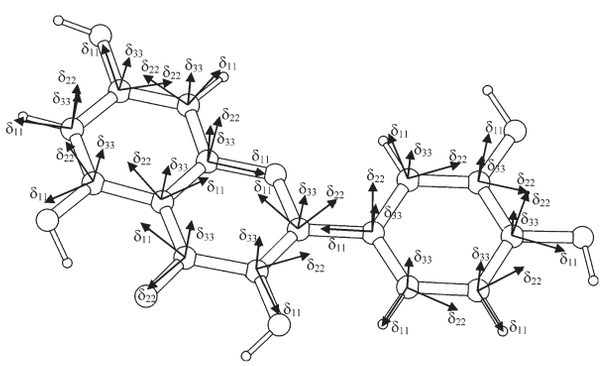

Fig. 10 Orientation of CST parameters *versus* molecular frame of sample **1**. The appropriate angles defining the orientation of ^{13}C δ_{ii} were obtained by means of theoretical DFT calculation with the B3PW91 functional and 6-311G** basis set.

Discussion

Although so far attention was mostly focused on the *anti* isomer of quercetin very recent theoretical DFT calculations unambiguously prove that the *syn* conformer is more favorable in the gas-phase and in water.[7] Our studies based on advance analysis of calculated NMR shielding parameters and supported by experimental data suggest the presence of the *syn* conformer in the condensed phase. The molecular structure of the *anti* isomer is apparent from X-ray studies.[8] As already discussed, in the crystal lattice quercetin forms a dihydrate. The presence of water seems to be a crucial factor determining the molecular geometry of quercetin. The intermolecular hydrogen bonds between water and OH groups of C3′, C4′ and C7 force their orientations in the crystal lattice. According to the notation discussed in the previous section the appropriate torsional angles Θ_1, Θ_2, Θ_3, Θ_4 are 175.01°, 165.64°, 176.92° and 175.28° respectively. Our results reveal that lack of water changes dramatically the phase organization of quercetin. We assumed that for the unhydrated form, the O3′–H group is involved in the formation of an intramolecular hydrogen bond with the O4′ atom of the B ring. Csizmadia and coworkers recently discussed the conformation of selected flavones, 5,7-dihydroxyflavone (chrysin) and 7,8-dihydroxyflavone in terms of intramolecular HB.[23] *Ab initio* and DFT calculations clearly proved that sparsely placed hydroxyl groups, particularly with hydrogen bond-like interactions resulted in lowering the potential energy minimum for the molecules. This conclusion is also valid for quercetin. Table 4 shows computed energies for structures **I–IV** (Scheme 2). It is apparent that intramolecular hydrogen bonding contributes to stabilization of the structure. The role of 3′ and 4′ hydroxyl groups and their influence on antioxidant properties of quercetin were discussed elsewhere. Kuhlmann *et al.* analyzing the radicals of quercetin and its structural analogues concluded that "protective activity of querectin is related to the presence of two hydroxyl groups in 3′- and 4′-position of the B ring and a hydroxyl in 3-position of C-ring in conjunction with a C2–C3 double bond of the basic flavone moiety."[24] Analysis of calculated ^{13}C σ_{ii} parameters proves that alignment of hydroxyl groups of the B ring has significant influence on σ_{22} values of C2′ and C6′ carbon atoms (see bold values in Table 1). In the previous section we showed that these parameters, oriented in the ring plane reflect the aromatic character of the compound. The distinction of σ_{ii} parameters for aromatic carbons can be rationalized in terms of relative differences in the electron density induced by the change of geometry and hydrogen bonding. The bond populations were calculated for the optimized structures of quercetin at the *ab initio* level employing a standard Mulliken formalism.[15] The calculated bond orders (BO) are displayed in Fig. 11. As seen, there are significant differences between BO for individual conformers. It is worth remembering that in this approach, the estimated C–C bond population is 0.27 for ethane, 0.57 for ethylene and 0.50 for benzene. Discussing the problem of aromaticity of quercetin, in the context of the NMR shielding of C2′ and C6′ atoms we have to consider the surrounding atoms under discussion and further BO for C1′–C2′, C2′–C3′ and C1′–C6′, C6′–C5′. Analysis of bond order parameters for the structures displayed in Fig. 11 shows significant differences. Conformer **I** with Θ_1, Θ_2, Θ_3 and Θ_4 torsion angles equal to 180° presents a large disparity of BO which gives 20 ppm difference between σ_{22} parameters for C2′ and C6′. On the other hand the *syn* conformer (**II**) with $\Theta_2 = 180°$ and $\Theta_3 = 180°$ is represented by very similar values of BO parameters for all carbons of the B ring. In consequence, the difference of σ_{22} between C2′ and C6′ is smallest among all the discussed conformers (6 ppm). It is interesting to note that for **II** despite very similar BO values the distinction of ^{13}C σ_{iso} is still observed (3 ppm). Although the conformer **III** shows a larger distinction of BO compared to **II** and the difference between σ_{22} is 10 ppm this conformer represents indeed a system with almost equal σ_{iso} values for C2′ and C6′. Inspection of ^{13}C σ_{ii} parameters clearly shows that a slightly larger distinction of σ_{22} is compensated by σ_{11} and σ_{33} parameters. Finally, two features require additional comment. First the intramolecular hydrogen bonding has significant influence on the BO of C3′–C4′. In each case the bond order is smaller compared to samples without such interactions. Second, the BO for the nominally single bond C2–C1′ is larger than the predicted theoretical value of 0.27. This bond has partial double bond character. For the *syn* conformer with intramolecular HB the value of BO of 0.333 suggests that stabilization effect will be strongest for structure **IV**.

In the final part of this work we wish to return to the problem of correlation between experimental values of CST parameters and calculated NMR shielding. Such a comparison is most diagnostic for sample **1**, for which the X-ray data is known and certainly NMR spectroscopy and the theoretical approach describe exactly the same geometry including also the local environment. From analysis of data collected in Table 3 and Fig. 9 it can be concluded that with small exceptions the correlation is very good. The exception regards mostly the C4 carbonyl group. The skew parameter expressed by the equation $\kappa = 3(\delta_{iso} - \delta_{22})/\Omega$ reflects the electron distribution for the desired nucleus. Ω (span) given by the equation ($\Omega = \delta_{11} - \delta_{33}$) describes anisotropy.[25] The experimental κ value for C4 is −0.74 while the calculated value employing theoretical ^{13}C δ_{ii} parameters

Table 4 SCF energies in arbitrary units for different conformers of quercetin. For used notation see Scheme 2

	I	II	III	IV
E/AU	−1104.0471	−1104.0475	−1104.0530	−1104.0526

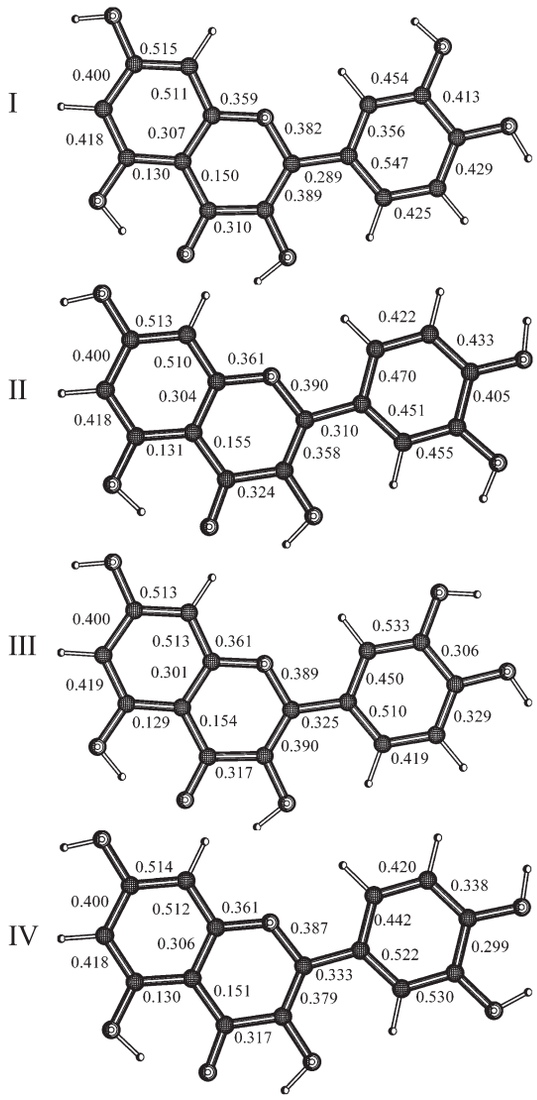

Fig. 11 Calculated bond order parameters for different conformers of quercetin.

is found to be −0.29. This distinction can be explained in terms of strong intramolecular hydrogen bonding with the carbonyl group as acceptor and the hydroxyl group at C5 as donor. According to X-ray data the distance between the O4 and O5 atoms is 2.576 Å. The appropriate O4 and C3 length is 2.711 Å.[8] It is known that very strong hydrogen bonds have a quasi-covalent character.[26]

In such a three-center four-electron bond, the H atom is involved in two partial covalent bonds of comparable bond order. It is noteworthy that theoretical calculations of NMR shielding parameters carried out on models with decreasing distance between H5 proton and O4 oxygen clearly prove the tendency to diminish distinction between σ_{11} and σ_{22} parameters for C4. The decreasing of σ_{22} values is compensated by increasing of σ_{11}. In consequence the isotropic chemical shifts show a very small deviation from the starting value. This feature in pictorial form is presented in Fig. 12.

Conclusion

To the best of our knowledge in this work we present the first comparative analysis of two crystallographic modifications of quercetin. The existence of dihydrate and unhydrated forms of quercetin in the condensed phase is confirmed by several experimental techniques *e.g.* X-ray diffraction of powders, DSC TGA and NMR. Our studies allow understanding of the complexity of quercetin samples obtained from different sources. It is clear that in many cases quercetin is provided as mixture of the unhydrated and dihydrated forms (see sample **2**).

Moreover, we have demonstrated here the complementarity and the power of the multi-technique approach in structural studies

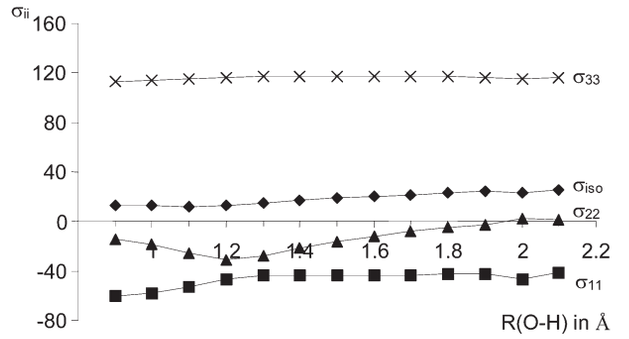

Fig. 12 Computed changes of ^{13}C NMR shielding parameters σ_{ii} for C4 carbonyl group *versus* the O5–H distance. The smallest distinction of σ_{11} and σ_{22} elements is seen for an O–H length of 1.2–1.3 Å.

of quercetin. Solid state NMR spectroscopy and DFT GIAO calculations provide unique information about NMR shielding and electron density distribution for different conformers. Theoretical calculations of NMR parameters for different spatial arrangements of the aromatic rings and geometry of the hydrogen bonds are found to be an invaluable tool, which allow us to rationalize the distinction of the spectral data. The changes of conformation and hydrogen bonding pattern have great influence on the aromaticity of quercetin. This conclusion has practical importance. As discussed elsewhere the antioxidant power of quercetin may be correlated mainly with ring B.[5,6] Our studies clearly prove that a small perturbation of geometry has great influence on bond orders of ring B. It can significantly change susceptibility for formation of radicals and in consequence biological properties of quercetin conformers.

Finally, we wish to emphasize that despite the fact that theoretical calculations and NMR experiments give a very consistent picture of the structure of quercetin conformers we still are looking for stronger proofs confirming the presence of *syn* quercetin. Such evidence can be obtained from single crystal X-ray diffraction studies. Unfortunately, to date our attempts to grow up a single crystal with quality suitable for X-ray measurements failed.

Experimental

The solid-state CP MAS ^{13}C NMR experiments were performed on a BRUKER Avance DSX 300 spectrometer at 75.47 MHz frequency, equipped with a MAS probehead using 4 mm ZrO_2 rotors. A sample of glycine was used for setting the Hartmann–Hahn conditions and adamantane as a secondary chemical shift reference δ = 38.48 ppm and 29.46 ppm from external TMS.[27] The conventional spectra were recorded with a proton 90 degree pulse length of 3.5 μs and a contact time of 1 ms. The repetition delay was 10 s and the spectral width was 25 kHz. The FID's were accumulated with a time domain size of 2K data points. The RAMP shape pulse was used during the cross-polarization and TPPM with τ_p 6.8 μs and a phase angle of 20° during the acquisition. The spectral data were processed using the WIN-NMR program.[28]

A sample spinning speed of 2 kHz was used in the PASS-2D experiments. The 16-point experiment data t_1 were replicated to 256 points. One-dimension CSA spinning sidebands were obtained from t_1 slices taken at isotropic chemical shifts in the ω_2 dimension of the 2D spectrum. The magnitudes of the principal elements of the CSA were obtained from the best-fitting simulated spinning patterns. Simulations of the spinning CSA sideband spectra were carried out on a PC using the SIMPSON program under LINUX environment.

DFT GIAO calculations were carried out with the GAUSSIAN 98 program running on a Silicon Graphics Power Challenge computer. The GIAO method with the B3PW91 hybrid method and 6-311++G** basis set was used to calculate geometry and NMR parameters.

DSC and TGA measurements were carried out on TA instruments, 2920 Modulated DSC and Hi-Res TGA 2950 Analyzer.

The X-ray intensity data were collected on a Siemens D5000 automatic powder diffractometer with a continous normal coupled ω–2θ scan mode. The 2.0 seconds per step exposure time was used, and

data were collected up to $2\theta = 90.000°$ with $2\theta = 0.040°$ scanning step. A Ni-monochromated Cu-Kα radiation ($\lambda = 1.54178$ Å) was used and the measurements were carried out at room temperature 293.0(2) K. The Diffrac AT v. 3.0 and Eva v. 3.09 software were used for data collection and data processing respectively.

Acknowledgements

The authors are grateful to the Polish Committee for Scientific Research, KBN, grant no. 3T 09A 02026.

References

1 S. A. Aherne and N. M. O'Brien, *Nutrition (Syracuse, NY)*, 2002, **18**, 75.
2 C. A. Rice-Evans, N. N. J. Miller and G. Paganga, *Free Radical Biol. Med.*, 1996, **20**, 933.
3 N. Russo, M. Toscano and N. Uccella, *J. Agric. Food Chem.*, 2000, **48**, 3232.
4 S. Erkoç, F. Erkoç and N. Keskin, *THEOCHEM*, 2003, **631**, 141.
5 S. A. B. E. van Acker, M. J. de Groot, D.-J. van der Berg, M. N. J. L. Tromp, D. G.-O. Kelder, W. J. F. van der Vijgh and A. Bast, *Chem. Res. Toxicol.*, 1996, **9**, 1305.
6 D. Vasilescu and R. Girma, *Int. J. Quantum Chem.*, 2002, **90**, 888.
7 M. Leopoldini, T. Marino, N. Russo and M. Toscano, *Theor. Chem. Acc*, 2003, **111**, 210.
8 (*a*) M. Rossi, L. F. Rickels and W. A. Halpin, *Bioorg. Chem.*, 1986, **14**, 55; (*b*) G.-Z. Jin, Y. Yamagata and K.-I. Tomita, *Acta Crystallogr., Sect. C*, 1990, **46**, 310.
9 I. Wawer and A. Zielińska, *Solid State Nucl. Magn. Reson.*, 1997, **10**, 33–38.
10 G. Metz, X. Wu and S. O. Smith, *J. Magn. Reson., Ser. A*, 1994, **110**, 219.
11 A. W. Bennett, C. M. Rienstra, M. Auger, K. V. Lakshmi and R. G. Griffin, *J. Chem. Phys.*, 1995, **16**, 103.
12 (*a*) M. Alla and E. Lippmaa, *Chem. Phys. Lett.*, 1976, **37**, 260; (*b*) S. J. Opella and M. H. Frey, *J. Am. Chem. Soc.*, 1979, **37**, 260; (*c*) K. W. Zilm, in: Spectral Editing Techniques: Hydrocarbon Solids, *Encyclopedia of NMR*, eds. D. M. Grant and R. K. Harris, John Wiley & Sons Ltd., Chichester, 1996, vol. VII, p. 4498.
13 eds. D. M. Grant, J. C. Facelli, D. W. Aldermanm, M. H. Sherwood and J. A. Tossell, *Nuclear Magnetic Shielding and Molecular Structure*, Kluwer Academic Publishers, Netherlands, 1993, p. 367.
14 V. G. Malkin, O. L. Malkina, L. A. Eriksson and D. R. Salahub, Modern Density Functional Theory: A Tool for Chemistry, in: *Theoretical and Computational Chemistry*, eds. J. M. Seminaro and P. Politzer, Vol. 2, Elsevier, Amsterdam, 1995.
15 *Gaussian 98*, Revision A.6, M. J. Frisch, G. W. Trucks, H. B. Schlegel, G. E. Scuseria, M. A. Robb, J. R. Cheeseman, V. G. Zakrzewski, J. A. Montgomery, Jr., R. E. Stratmann, J. C. Burant, S. Dapprich, J. M. Millam, A. D. Daniels, K. N. Kudin, M. C. Strain, O. Farkas, J. Tomasi, V. Barone, M. Cossi, R. Cammi, B. Mennucci, C. Pomelli, C. Adamo, S. Clifford, J. Ochterski, G. A. Petersson, P. Y. Ayala, Q. Cui, K. Morokuma, D. K. Malick, A. D. Rabuck, K. Raghavachari, J. B. Foresman, J. Cioslowski, J. V. Ortiz, B. B. Stefanov, G. Liu, A. Liashenko, P. Piskorz, I. Komaromi, R. Gomperts, R. L. Martin, D. J. Fox, T. Keith, M. A. Al-Laham, C. Y. Peng, A. Nanayakkara, C. Gonzalez, M. Challacombe, P. M. W. Gill, B. Johnson, W. Chen, M. W. Wong, J. L. Andres, C. Gonzalez, M. Head-Gordon, E. S. Replogle and J. A. Pople, Gaussian, Inc., Pittsburgh PA, 1998.
16 (*a*) J. Hu, W. Wang, F. Liu, M. S. Solum, D. W. Alderman and R. J. Pugmire, *J. Magn. Reson., Ser. A*, 1995, **113**, 210; (*b*) D. W. Alderman, G. McGeorge, J. Z. Hu, R. J. Pugmire and D. M. Grant, *Mol. Phys.*, 1998, **95**, 1113; (*c*) L. Frydman, G. C. Chingas, Y. K. Lee, P. J. Grandinetti, M. A. Eastman, G. A. Barral and A. Pines, *J. Chem. Phys.*, 1992, **97**, 480; (*d*) A. C. Kolbert and R. G. Griffin, *Chem. Phys. Lett.*, 1990, **166**, 87.
17 O. N. Antzutkin, *Prog. Nucl. Magn. Reson. Spectrosc.*, 1999, **35**, 203.
18 O. N. Antzutkin, S. C. Shekar and M. H. Levitt, *J. Magn. Reson.*, 1995, **115**, 7.
19 W. T. Dixon, *J. Chem. Phys.*, 1982, **77**, 1800.
20 M. Bak, J. T. Rasmussen and N. C. Nielsen, *J. Magn. Reson.*, 2000, **147**, 296.
21 F. Liu, D. W. Phung, D. W. Alderman and D. M. Grant, *J. Am. Chem. Soc.*, 1996, **118**, 10629.
22 D. M. Grant, *Chemical Shift Tensors In Encyclopedia of NMR*; eds. D. M. Grant and R. K. Harris, John Wiley & Sons Ltd., Chichester, 1996, vol. IV, p. 1298.
23 K. S. Lau, A. Mantas, G. A. Chass, F. H. Ferretti, M. Estrada, G. Zamarbide and I. G. Csizmadia, *Can. J. Chem*, 2002, **80**, 845.
24 M. K. Kuhlmann, G. Burkhardt, E. Horsch, M. Wagner and H. Kohler, *Free Radical Res*, 1998, **29**, 451.
25 J. Mason, *Solid State Nucl. Magn. Reson.*, 1993, **2**, 285.
26 G. R. Desiraju, *Acc. Chem. Res.*, 2002, **35**, 565.
27 C. R. Morcombe and K. W. Zilm, *J. Magn. Reson.*, 2003, **162**, 479.
28 *Win-NMR, Bruker-Franzen Analytik GmbH*, Version 6.0, Bremen, Germany, 1993.